THE JOURNAL OF PHYSICAL CHEMISTRY A

Article

Electronic Structure and Reactivity of Cobalt Oxide Dimers and their Hexacarbonyl Complexes: a Density Functional Study

Ellie Uzunova, and Hans Mikosch

J. Phys. Chem. A, **Just Accepted Manuscript** • DOI: 10.1021/jp3006052 • Publication Date (Web): 07 Mar 2012

Electronic Structure and Reactivity of Cobalt Oxide Dimers and their Hexacarbonyl Complexes: a Density Functional Study

Ellie L. Uzunova [a], *Hans Mikosch* [b]

[a] Institute of General and Inorganic Chemistry, Bulgarian Academy of Sciences, Acad. G. Bonchev Str., bl. 11, Sofia 1113, Bulgaria; [b] Institute for Chemical Technologies and Analytics, Vienna University of Technology, Getreidemarkt 9/E164/EC, A-1060 Vienna, Austria

ellie@svr.igic.bas.bg

ABSTRACT

The dimers of cobalt oxide $(CoO)_2$ with cyclic and open bent structure are studied with the B1LYP density functional; the ordering of states is validated by the CCSD(T) method. The D_{2h}-symmetry rhombic dioxide Co_2O_2 with antiferromagnetically ordered electrons on cobalt centers is the global minimum. The cyclic peroxide $Co_2(O_2)$ with side-on bonded dioxygen in $^7B_2$ ground state is separated from the global minimum by an energy gap of 3.15 eV. The dioxide is highly reactive as indicated by the high value of proton affinity and chemical reactivity indices. The four-member ring structures are more stable than those with three-member ring or chain configuration. The thermodynamic stability towards dissociation to CoO increases upon carbonylation, whereas proton affinity and reactivity with release of molecular oxygen also increase. The global minimum of $Co_2O_2(CO)_6$ corresponds to a triplet state ^3A" with oxygen atoms shifted above the molecular plane of the rhombic dioxide Co_2O_2. The

SOMO-LUMO gap in the ground state carbonylated dioxide is wider, compared to the same gap in the bare dicobalt dioxide. The peroxo-isomer $Co_2(O_2)(CO)_6$ retains the planar $Co_2(O_2)$ ring and is only stable in a high-spin state ^{7}A". The carbonylated clusters have increased reactivity in both redox and nucleophilic reactions, as a result of the increased electron density in the Co_2O_2-ring area.

Keywords: Electronic Structure; Magnetic Structure; Density Functional Calculations; Cobalt oxide dimers; Carbonyl Complexes

INTRODUCTION

The binuclear coordination compounds of the 3d elements participate in many organic and bio-organic reactions and they find applications in organometallic chemistry, photochemistry and homogeneous catalysis. [1,2] In many catalytically active coordination compounds, the active sites are also stable as small clusters, which can be studied by theoretical and experimental methods. [3] The small cluster dimers of transition metal monoxides are of major interest, because they are formed at the first step of the growth of nanoparticles and some configurations correspond to active sites in heterogeneous catalysts. [1-5] In the studies of such clusters theoretical methods provide valuable insight, as the experimental data available cannot present direct evidence for the structure, the ground states and the relative ordering by energy. The computational studies also face challenges, because of the large number of possible electronic states, near-degeneracy problems and complicated magnetic ordering. [4] The 3d elements form binuclear clusters M_2O_n (n=1-6) with molecular oxygen and the four-member ring structures $(M_2O_2)O_{n-2}$ dominate among the possible isomers. [5,6] A higher stability towards release of either molecular or atomic oxygen was found for Cr_2O_2 among the CrO_m and Cr_2O_m clusters with $1< m < 3$. [6] Among the monocations $Fe_nO_m^+$ with ($n< 6$, $n \leq m$), those with Fe/O ratio 1:1, $(FeO)_n^+$, proved to be of the highest stability. [7] Ionic species $Co_2O_2^+$ and $Co_2O_2^-$ were formed with high yield in reactions of laser-ablated Co atoms with dioxygen. [5,8] Both atomic Co and the dimer Co_2 possess numerous low-lying excited states; [9-11] this applies to oxide clusters Co_nO and CoO_n (n=2-4) as well. [12,13] The averaged atomic binding energies were found to increase significantly from CoO to Co_2O, and keep a constant trend by further increasing the number of metal atoms. [12] The $(CoO)_2$ clusters, formed as reaction products of laser-ablated cobalt atoms and molecular oxygen have been studied by IR spectroscopy as isolated species in solid Ar, N_2 and Ne matrices. [14] In the latter study, a rhombic planar cluster was denoted as the lowest energy structure. While experimental and theoretical studies agreed on the structure of the most stable cobalt oxide dimer as a rhombic planar cluster, its magnetic state has not been ascertained and little is known about the less stable structural isomers. Cobalt oxide is known as

both active catalyst and a support and the nano-structured species certainly exhibit high activity and selectivity in a variety of industrially relevant catalytic processes. The binding of dioxygen has a strong impact on catalytic performance: the type of species (O^{2-}, O_2^{2-} or O_2^{-}) and the metal-oxygen bond strength determine the activity and selectivity; the transition metal centers should also easily be reoxidized to avoid deactivation. [15] Peroxide-isomers $Co_2(O_2)$ with Co-Co bond and side-bonded oxygen atoms have not been examined by theoretical studies yet, though low-symmetry structures have been detected in the matrix-isolation studies. The redox potentials, the stability and reactivity of binuclear oxo-clusters are broadly tunable by the coordination of ligands. The dicobalt octacarbonyl and the dicobalt hexacarbonyl are known as catalysts for the Nicholas reaction and find application in a number of reactions in organic synthesis [15e]; the dicobalt dioxygen clusters with coordinated carbonyl ligands are promising as a model system for a water oxidation catalyst.

The low-energy minima of the $(CoO)_2$ neutral, positive and negatively charged clusters as well as the dications and dianions are subject of the present study. The clusters in which Co atoms are bonded via bridging oxygen atoms (2 Co-O-Co linkages), and their isomers with peroxide bridging bond separating the Co atoms (Co-η^1-OO-η^1-Co linkages), as well as isomers with side-bonded dioxygen to Co dimers (Co_2-η^2-(O_2) and Co-μ-(O_2)-μ-Co linkages), are examined by density functional theory (DFT) and the coupled cluster method with the aim to study their relative stability, bonding scheme and the ordering by energy of their electronic states with different spin multiplicities. All possible isomers with Co_2O_2 stoichiometry were considered, including low-symmetry clusters containing three-member rings or chain-like configurations. The vibrational frequencies in the gas-phase and in an inert-gas matrix, the local magnetic properties, the charge density distribution, and the proton and electron affinity of the neutral species are assessed. The effect of carbonyl ligands coordination on the electron-donor properties, the stability and reactivity of Co_2O_2 clusters with different structure is examined.

Methods

Computational Methods. All calculations were performed with the B1LYP method, which includes local and non-local terms as implemented in the Gaussian 09 package. [16-21] The Becke one-parameter functional is closely related to the B3LYP functional, [17,21] the three parameters being substituted by one. In B1LYP the ratio between Hartree-Fock and density functional exchange is determined *a priori* from purely theoretical considerations and no further parameters are present. [18] The standard 6-311+G(d) basis set with diffuse and polarization functions was employed, which consists of the Wachters-Hay all electron basis set for the first transition row, using the scaling factors of Raghavachari and Trucks. [23] In terms of atomic orbitals, the basis set is represented as [10s7p4d1f] for the 3d element, [5s4p1d] for oxygen and [5s9p5d7f] for Ar. Regarding the optimized geometries of the ground states, expanded basis set, 6-311+G(2df), produced essentially the same results with maximal deviation in bond lengths of ±0.006 Å and 0.4° in bond angles; this basis set however, is too expensive for CCSD(T) calculations and for optimizations in the Ar cell. The minima on the potential energy surfaces for the allowed spin multiplicities were identified by the absence of negative eigenvalues in the diagonalized Hessian matrix. Spin contamination expectation values $\langle \hat{S}^2 \rangle$ were estimated by treating the DFT orbitals as single-determinant Hartree-Fock wave functions. The deviation of $\langle \hat{S}^2 \rangle$ from the ideal value $S(S + 1)$ where S denotes the total spin of the electronic system provides the degree of spin contamination. Singlet states were examined in spin-unrestricted mode and calculations in the broken symmetry (BS) approach were performed. [25,44] The antiferromagnetic (AFM) coupling of electrons on Co centers was examined for the fixed spin component $S_z = 0$ (singlet), 1 (triplet), 2 (quintet). The BS approach consists in the localization of the opposite spins on different parts of the molecule to give a mono-determinant representation of the spin exchange interactions within the molecule which reduces the symmetry of the space and spin wavefunctions with respect to that of the nuclear framework. The BS wavefunction is not a pure spin state; it is an eigenstate of S_z, but not of $\hat{S}^2$. Noodleman showed that the BS state is a weighted average of pure-spin wavefunctions and that correspondingly the BS state energy is a

weighted average of pure spin state energies. We have used the spin magnetization density (SMD) distributions $m_s(r) = \rho_\alpha(r) - \rho_\beta(r)$, where ρ_α and ρ_β denote α and β spin densities, to ascertain the antiferromagnetic character of the calculated broken-symmetry singlet states. Coupled-cluster singles and doubles, including non-iterative triples, CCSD(T) [26] single-point calculations have been performed with the B1LYP-optimized geometries for the ground state and the low-lying excited states. Vibrational frequencies were calculated also for oxide clusters encaged in a solid Ar cell. The calculations were performed with four Ar atoms from the solid Ar supercell accommodating one Co_2O_2 cluster and full relaxation was allowed. The frequencies of the imaginary vibrations, due to the incomplete cluster model and arising from movements of the Ar framework atoms, did not exceed in absolute values 20 cm^{-1}. The Ar-encaged models were examined also via the double-hybrid density functional B2PLYPD, [22] which includes a second-order perturbation correction for non-local correlation effects and dispersion correction. The latter calculations are considerably more expensive and they were performed with the Los Alamos basis set and core-effective potential LANL2DZ with optimized outer p-functions applied to the Co atoms. [24] AFM calculations however, proved to be too expensive for the B2PLYPD method. The bond populations and charge distributions were examined by natural bond orbital (NBO) analysis. [28] This method yields results that are rather insensitive to basis set enlargement and reveals both covalent and non-covalent effects in molecules. Magnetic moments at the atoms (μ) were calculated as a difference between α and β natural populations. The electrostatic potential (ESP) of the clusters was calculated from the B1LYP density and molecular orbital maps and molecular electrostatic potential (MEP) maps were derived in which areas of enhanced reactivity in the various clusters can be discerned. Pearson absolute electronegativity (χ) and hardness (η) were calculated according to the formulas $\chi = (I + A)/2$; $\eta = (I - A)/2$, where I denotes the ionization energy and A is the vertical electron affinity. [36]

Validation of Methods: Cobalt oxide, cobalt dimers and the oxygen species. The reliability of the method and the basis set applied in the present study were tested by calculating properties of cobalt

monoxide, dimeric cobalt and dioxygen species, for which experimental data are available, Table 1S (Supporting Information). [10, 29-33] B1LYP yields essentially the same results as B3LYP, at lower cost of computer time and our calculations on ground-state Co_2O_2, $Co_2(O_2)$ and CoOOCo clusters, as well as their carbonyl complexes confirmed this (Tables 2S, 3S and 4S in the Supporting Information). A very good agreement with experimental data is obtained for the B1LYP calculated CoO bond length, dissociation energy and adiabatic electron affinity of the ground state, $^4\Delta$. The use of the meta-GGA functional TPSS [27] yields also very satisfactory results, except for the CoO dissociation energy, which is overestimated by about 0.5 eV (4.417 eV vs 3.94±0.14 eV exp.), in the same way as the BPW91 functional does. [34a] The B1LYP calculated electron affinity of O_2 (0.435 eV) is also in excellent agreement with experiment, Table 1S. The experimental data on Co dimers are scarce, the dissociation energy being somewhat contradictory - 1.69 eV [33a] versus less than 1.32 eV [33b] and the B1LYP calculated value is 0.681 eV. The Co_2 ground state is $^5\Delta_g$ and the B1LYP calculated electron affinity is 0.808 eV, thus it is below the experimental value of 1.110±0.008 eV, while the electron affinity of atomic cobalt is slightly overestimated. The T_1 diagnostics values for examined clusters have been determined according to the criterion of Lee and Taylor, [39] based on the Euclidian norm of the t_1 vector of the coupled-cluster singles and doubles wave function. For the CoO dimers they were found in the range 0.04-0.06, being smaller for the high-spin states. These values are comparable with the T_1 diagnostics values for the metal monoxide clusters of the 3d elements, ranging from 0.04 to 0.05 for ScO, TiO and CuO, and though they reach 0.09-0.10 for MnO to NiO, the monoxides are well described by DFT with either the B1LYP or the B3LYP functionals. [34b,d] Moderate spin-contamination was detected for the ground-state monoxides of the elements from Mn to Cu; this also affects the T_1 diagnostic values for the CCSD wavefunction.

Structure and Bonding of Neutral and Charged $(CoO)_2$ and of the Peroxide Clusters $Co_2(O_2)$ and CoOOCo

Dioxides. The planar rhombic dioxide clusters $(CoO)_2$ with D_{2h} symmetry are the dominant species in the low-energy part of the allowed multiplicity channels among all studied isomers with Co_2O_2 stoichiometry according to the B1LYP and CCSD(T) results, Figure 1. Dicobalt dioxide was subject of theoretical studies using different methods. [5,14,35] The ^7A_u state was suggested as the most stable one in earlier B3LYP studies performed with a smaller basis set on oxygen atoms and a $^5B_{3u}$ state with similar structure was found at 7 kcal mol^{-1} above the ground state. [14] Antiferromagnetic $(CoO)_2$ in singlet ground state was found with the PW91 functional, while high-spin ground state was deduced for the monocation, $(CoO)_2^+$. [5] In the broken-symmetry approach, calculations with the TPSS density functional also found antiferromagnetic singlet ground state for the rhombic dioxide. [35a] Strong antiferromagnetic coupling was inferred, with the spin moments of three unpaired electrons on one cobalt atom having anti-parallel orientation to the three unpaired electrons on the other cobalt atom. Very small energy gaps between the antiferromagnetically ordered singlet state and the higher-spin broken-symmetry states were reported in the same study – about 3 kcal mol^{-1} – which is below the zero-point energy for these clusters. Such small energy gaps would allow interconversion between states and spin-flipping. The present B1LYP and CCSD(T)//B1LYP study reveals an antiferromagnetic singlet ground state of the planar rhombic $(CoO)_2$ in agreement with the previous PW91 and TPSS calculations, Table 1. This cluster is found to be at 0.91 eV below the ^7A_u state and by 0.24 eV below the $^7B_{1u}$ state. The antiferromagnetic ordering involves predominantly the Co centers, which bear a local magnetic moment of 2.57 μB. The first adiabatic ionization energy of $(CoO)_2$ determined at the B1LYP level is very high, 9.015 eV; it corresponds to the formation of a rhombic monocation in $^6B_{2g}$ state and indicates that despite the presence of a bond Co-Co, the clusters bear typical oxide features. The second adiabatic ionization energy is 14.476 eV, and the planar dication is stabilized by antiferromagnetic coupling. The $(CoO)_2$ calculated adiabatic electron affinity of 1.172 eV is considerably smaller than the electron

affinity of either CoO or CoO_2, for which experimental data are available. [13,30] In the dianions, the antiferromagnetic coupling involves only the Co centers as in the neutral cluster, with local magnetic moments reaching 3.77 μB, while in the dications, the oxygen centers also bear an unpaired electron. Examination of the spin magnetization density distribution clearly shows the antiferromagnetic character of the broken-symmetry singlet states, Figure 2. An oxide cluster with a three-member ring (Co-O-Co)O was found in non-planar configuration, with a terminal Co=O bond pointing out of the ring plane. This cluster is stable only in ^1A state and the Co atoms bear no magnetic moment; it does not exist in higher-spin states and lies at higher energy than the four-member ring oxides and the ground state peroxides, Figure 1. Ionic structure can be assigned to the rhombic neutral dioxide $(CoO)_2$, evidenced by the charge distribution, Table 2. Upon formation of dications, the negative charge on oxygen atoms decreases, while the charge on Co atoms undergoes moderate augmentation. Conversely, the formation of dianions mainly affects the charge on Co atoms. The formation of a monoanion is accomplished with minor energy gain, as evidenced by the moderate electron affinity, and the rhombic dianions are less stable than the corresponding neutral clusters. The attachment of two electrons leads to shortening of the Co-Co bond, while in the dications the Co-Co bond is lengthened. The Co-O bond does not experience significant change upon formation of dianions; in the ground state dication it is shortened by 0.07 Å, Table 1.

Peroxides. The peroxide isomers examined in the present study include $Co_2(O_2)$ with side-on bonded dioxygen to a Co-dimer (C_{2v} symmetry), and CoOOCo with a peroxo-bond connecting the two cobalt atoms (C_{2h} or C_1 symmetry), Figure 1. All of the peroxide clusters lie at higher energies than the dioxides, but the planar four-member ring configurations are of higher stability than those with chain structure or containing three-member rings. The ground state $Co_2(O_2)$ cluster with side-on bonded dioxygen to the Co-dimer in its $^7B_2$ ground-state is a planar four-member ring, lying at 3.15 eV above the global minimum. No stable quintet states of $Co_2(O_2)$ were found, but the C_{2h} symmetry peroxide CoOOCo with a bridging peroxo-bond and chain configuration has a quintet ground state ^5A_g, which

lies at 0.33 eV above the $^7B_2$ state of the cyclic planar peroxide with side-on bonded dioxygen; unlike the latter one, it does not contain a Co-Co bond. The triplet and singlet states of $Co_2(O_2)$ lie at much higher energy above the $^7B_2$ ground state and so does the planar peroxide containing a three-member ring, (CoOO)O in $^1A'$ state. The CCSD(T) calculations indicate even a higher energy gap between the septet ground state and the $^3A_2$ or $^1A_1$ states of $Co_2(O_2)$, the latter two appearing as nearly iso-energetic, Table 1. A non-planar configuration with the dioxygen oriented perpendicular to the Co-Co axis is also a local minimum and a small energy gap of 25.2 kJ mol^{-1} separates it from the $^7B_2$ ground state of the planar cluster. Such a small energy gap is comparable to the zero-point energy of $Co_2(O_2)$, 14.5 kJ mol^{-1} and rotation of the dioxygen fragment would be easily achieved. The low-energy a_2 vibration (62 cm^{-1}) of $Co_2(O_2)$ corresponds to out-of-plane displacement of the oxygen atoms and this distortion brings the cluster into a non-planar structure Co-μ-(O_2)-μ-Co, again in $^7B_2$ state and with C_{2v}-symmetry, but with different orientation of the peroxo-bond, Figure 3. In a similar way, the chain-structured peroxide of C_{2h} symmetry in ^5A_g state would easily undergo out-of-plane deformation by the a_u-vibration, forming a non-planar Co-η^1-OO-η^1-Co configuration (Figure 2S, Supporting Information).

Cluster reactivity. The dissociation energy of $(CoO)_2$ with release of molecular oxygen in the state of the global minimum (5.83 eV) is considerably higher than that of CoO_2 (2.13 eV). [13] A more favorable dissociation path is towards CoO formation, Table 3. The cobalt oxide dimer is highly reactive and acts both as an electrophile (at the Co centers) and as nucleophile (at the O centers), as indicated by the values of absolute electronegativity and hardness. The proton affinity of $(CoO)_2$ is higher than that of molecular oxygen (421.0 kJ/mol) or hydroxyl groups (593.2 kJ/mol). [38] The Co-Co internuclear distance in the neutral rhombic dioxides and in the peroxides with side-on bonded dioxygen varies in a broad range for the triplet, quintet and septet states, 2.25-2.58 Å. The shortest Co-Co bonds of 2.11 Å belong to the singlet state of the peroxide cluster and the singlet state of the dianion, which are of much lower stability, Table 1. The Co-O bonds are of lengths within 1.73-2.00 Å, the more lengthened bonds being found in the triplet states of the peroxide clusters and in the non-planar peroxides with side-on bonded

dioxygen, oriented perpendicular to the Co-Co bond. In the neutral dioxides and dioxide anions the O-O internuclear distances are longer than the Co-Co distances, while in the dications the Co-Co distances become smaller. In both the ring-type and chain-type peroxides, the O-O bonds have the typical lengths for peroxide compounds, 1.33-1.48 Å, but they are significantly lengthened to 1.52-1.57 Å in the non-planar peroxides. The peroxides are of much lower stability than the dioxides within each multiplicity channel and the energy gaps are larger than 2.2 eV, Figure 1. Despite the fact that the Co-Co bond in a Co_2 dimer is not a strong one and in the cobalt oxide dimers it is lengthened much more than in the metallic dimer monoanion $(Co_2)^-$ [9], the cyclic Co_2O_2 clusters which contain a Co-Co bond are of high stability. Attempts to optimize dioxide chain-like structures containing a Co-Co bond and separated oxygen atoms, resulted in the more stable cyclic configurations. The peroxo-isomers are largely covalent and 3d-4s orbital hybridization is indicated by the significantly occupied 4s orbitals, Table 2. In the peroxides, the SOMO-LUMO gap is considerably smaller as compared to dioxides, though larger than in the dioxide dianions. The effect of stabilization of the rhombic planar clusters by antiferromagnetic coupling is manifested by the significant increase of the HOMO-LUMO gaps. The non-planar peroxide isomer Co-μ-(O_2)-μ-Co in $^7B_2$ state has the same charge distribution and similar 3d,4s occupancy as the planar dioxide, from which it supposedly originates, but the SOMO-LUMO gap in the non-planar $Co_2(O_2)$ is much smaller, 2.21 eV. The $10a_g$ and $8a_g$ MOs of the $^7B_{1u}$ state dioxide $(CoO)_2$ are highly delocalized, they are composed by the d_{z^2} AOs of Co and the $O2p_y$ AOs. A δ-type bond with participation of $d_{x^2-y^2}$ Co AOs is represented by the $9a_g$ MO, Figure 4. The highly delocalized $7a_g$ orbital, comprised by O2s AOs, together with the $9a_g$ MO contribute to the increased electron density in the plane of the cluster. The SOMO orbital of cobalt peroxide, $Co_2(O_2)$ in the $^7B_2$ ground state, is also delocalized and its dominant contribution is in the Co-Co bond formation. A similar shape of the SOMO is observed in the carbonylated $Co_2(O_2)$ cluster (next paragraph). In the ^5A_g ground state of CoOOCo, the SOMO is the $5b_g$ MO, which is non-bonding and bears the features of an oxygen

lone-pair orbital. The LUMO in both the dioxides and the peroxides is a typically antibonding orbital. The molecular electrostatic potential (MEP) maps, calculated from the DFT density, indicate that in all cluster types the Co centers are highly electrophilic. The ionic character of Co_2O_2 and the higher local charge at oxygen atoms are not related to higher nucleophilicity of the oxide-type oxygen atoms, compared to the largely covalent peroxide clusters. A continuous area of increased electron density emerges in the vicinity of peroxide oxygen atoms, while separate nucleophilic areas are formed around each oxygen atom in the dioxides, Figure 5.

Structure and bonding of carbonylated dicobalt dioxide and peroxide

Each of the Co centers in the dioxides Co_2O_2 or the peroxides with side-on bonded dioxygen, $Co_2(O_2)$, coordinates up to three CO molecules, Figure 6. In the carbonylated dioxides $Co_2O_2(CO)_6$, the rhombic cores Co_2O_2 are no longer planar: the oxygen atoms lie above the Co-Co bond in the σ_h plane, which divides the two $Co(CO)_3$ fragments. Both the dioxides $Co_2O_2(CO)_6$ with distorted rhombic core Co_2O_2, and the peroxides $Co_2(O_2)(CO)_6$ with side-on bonded dioxygen, are of C_s symmetry. The deviation from planarity of the Co_2O_2 ring is more significant for the ground state ^{3}A" and for the ^{1}A' state, while in the ^{5}A" and ^{7}A' high-spin state clusters, the Co_2O_2 rings are nearly planar, Table 4. Carbonylation increases the thermodynamic stability towards fragmentation to CoO and also reduces the energy gaps between dioxide and peroxide configurations and between states with different multiplicity. The triplet state ^{3}A" is the global minimum and the next low-lying state is the BS singlet state with antiferromagnetically coupled electron spins on the Co centers. The AFM coupling involves mainly the Co_2O_2 core, but it is smaller than in the bare clusters and the ligands bear minor unpaired electron density, Figure 2. The BS singlet and the ground state ^{3}A" are nearly iso-energetic and have almost identical geometry, thus it could be expected that they coexist differing only in magnetic properties. The peroxide is only stable in the ^{7}A" state, with Co-O and Co-Co bonds significantly lengthened as compared to the bare, non-carbonylated clusters. The Co-O bonds undergo elongation

also in the carbonylated dioxides; the Co-Co bonds are strongly lengthened compared to the bare clusters within each multiplicity channel, except for the high-lying singlet states. The nearly planar Co_2O_2 rings in quintet and septet states are considerably distorted along the axis of the Co-Co bond. In the ^{7}A' state of the dioxide the two oxygen atoms become non-equivalent, the second atom being weakly bound to the Co atoms. Cobalt-carbon bonds have the typical features of binuclear carbonyls, with Co-C bond lengths varying within 1.880-2.000 Å; the carbon-oxygen bonds also have lengths commonly found in carbonyls, 1.128-1.140 Å. [40] CO is a typical σ-donor and forms linear M-CO bonds; π-dative bonding also occurs due to metal-to-ligand charge transfer (MLCT) and this results in population of the CO vacant π* antibonding orbitals. In the carbonylated rhombic dioxide clusters the CO bond lengthening is minor, 1.128 – 1.131 Å, compared to the calculated value of the free CO molecule (1.126 Å), which indicates small level of MLCT. The shape of the 40a' bonding orbital in $Co_2O_2(CO)_6$, however, indicates that this effect is not negligible, Figure 7. In the peroxide complex $Co_2(O_2)(CO)_6$, MLCT is more pronounced and the CO bond lengths vary within 1.132-1.140 Å, the two CO bonds in the $Co_2(O_2)$ plane being most lengthened. This is illustrated also by the shape of the SOMO orbital, Figure 8.

The magnetic moment on Co atoms in the carbonylated dioxide and peroxide clusters is smaller and corresponds to maximum of two unpaired electrons per Co atom in the septet states ^{7}A' and ^{7}A", Table 4. Spin density is relocated to the Co-bonded oxygen atoms, and to a much smaller extent, to carbon atoms. In the antiferromagnetic singlet state ^{1}A, the magnetic moment on each of the Co centers corresponds to one unpaired electron and the carbon atoms bear a minor magnetic moment (below 0.08 μB), while the oxygen anion centers remain diamagnetic, Figure 2c. Unlike the bare clusters, antiferromagnetic coupling does not stabilize the carbonyl complexes over their paramagnetic states. The effect of ligand-to-metal charge transfer (LMCT) is significant and results in inducing a negative partial charge on Co atoms, as well as in higher occupancy of the Co3d AOs, Table 2. In $Co_2O_2(CO)_6$ the Co-O bonds are largely covalent in contrast to the bare Co_2O_2, which bears typically ionic character.

The SOMO-LUMO gap increases in the carbonylated rhombic dioxide relative to the neutral bare dioxide cluster, but in the peroxide carbonylated cluster the SOMO-LUMO gap is considerably smaller compared to all other neutral clusters. The Co-O and O-O bonding molecular orbitals are closely related by shape to the corresponding orbitals of the bare Co_2O_2 and $Co_2(O_2)$; in the carbonylated clusters however, they are shifted by energy closer to the frontier orbitals. The Co-Co bonding orbitals are highly delocalised in both the dioxide and in the peroxide and an area of increased electron density is formed inside and around the Co_2O_2 ring, Figures 7 and 8.

Vibrational Frequencies and Cluster Reactivity.

The planar dioxides span the irreducible representation $\Gamma[Co_2O_2, D_{2h}] = 2a_g(R) + b_{3g}(R) + b_{1u}(IR) + b_{2u}(IR) + b_{3u}(IR)$ for $(CoO)_2$ positioned in the σ_{yz} plane and IR denoting infra-red active vibrations, R – Raman active. The highest frequency vibration corresponds to a symmetric displacement of the oxygen atoms in the plane of the molecule (a_g symmetry), leading to Co-O stretching, mixed with OCoO bending and it is only Raman active. The IR-active vibrations originate from the antisymmetric Co-O stretching (b_{1u}), the Co-O-Co bending (b_{2u}) modes, and the out-of-plane b_{3u} mode. For the dioxide Co_2O_2, the experimental IR frequencies in solid Ne and Ar are nearly identical, but a significant frequency shift was observed in solid nitrogen, thus interaction with the matrix can be suggested. The transition metals and transition metal oxides often interact strongly with atoms from the inert-gas matrix. [34,41-43] Coordination of one atom from the matrix to the transition metal center was reported for a number of mononuclear oxide clusters and molecular modeling indicated strong distortion of the nearest matrix environment as well. [34b,c] The hydrated cations of Mn and Cu were found to coordinate Ar atoms, the metal cation-to-Ar internuclear distances being longer for $Mn^+(H_2O)$, (> 3.330 Å) [43] and shorter for $Cu^+(H_2O)$ (2.322 Å; 2.778 Å). [42] Comparable short Cu-Ar internuclear distances were predicted by B1LYP calculations for the monoxide CuO in Ar matrix. [34b] According to the present study, a reasonable agreement with the spectral data was obtained for a cluster model including four atoms of

the solid Ar unit cell, Figure 9. In the optimized configuration Co_2O_2 coordinates two Ar atoms and the Co-Ar internuclear distances of 2.937 Å are shorter than the values found for the MO_3 clusters of M=Co and Ni, Table 5. [34c] The remaining two Ar atoms are found at Co-Ar distances longer than 4.2 Å. The Co centers in the peroxide also coordinate Ar atoms, but with much lengthened Co-Ar internuclear distances of 3.256 Å. The geometry of the Ar-encaged rhombic cluster in $^7B_{1u}$ state was confirmed by B2PLYPD calculations, but shorter Co-Ar bonds were predicted and the Co-Co and Co-O bonds were also by 7-8% shortened than in the B1LYP or B3LYP calculations. The normal modes of the planar dicobalt peroxide with side-on bonded dioxygen span the irreducible representation: $\Gamma[Co_2\text{-}\eta^2\text{-}(O_2), C_{2v}] = 3a_1(IR,R) + 2b_2(IR,R) + a_2(R)$. The number of IR-active vibrations remains the same for the non-planar peroxide cluster with irreducible representation $\Gamma[Co\text{-}\mu\text{-}(O_2)\text{-}\mu\text{-}Co, C_{2v}] = 3a_1(IR\ R) + b_1(IR,R) + b_2(IR,R) + a_2(R)$. The highest frequency vibration in the peroxo-clusters corresponds to the O-O stretching mode and it is found in the range 780-850 cm^{-1} for the ground state peroxides. The O-O vibration of the non-planar cluster $Co(O_2)Co$ appears in the lower-energy part of this range, Table 5S (Supporting information). The triplet states of peroxides in which the Co-O bonds are weaker, but the O-O bonds are stronger, have their stretching O-O modes shifted to 1100 cm^{-1} for the chain-type C_{2h}-symmetry clusters CoOOCo, and to 1200 cm^{-1} for the C_{2v}-symmetry peroxides $Co_2(O_2)$ with four-member planar ring structure. The O-O stretching mode is significantly shifted to higher energy in the carbonylated peroxide, due to the strengthened O-O bond, while other modes attributed to the $Co_2(O_2)$ core are shifted downwards as a result of the weakened Co-O bonds. Peroxides have not been unambiguously identified in the IR spectral studies, but the existence of metastable isomers of Co_2O_2 was reported. [14] Low-symmetry species with non-equivalent oxygen and/or cobalt atoms have been found in the high-energy part of the singlet multiplicity channel, Figure 1. A CoOCoO bent cluster with terminal Co-O bond was reported in experimental studies of the interaction of laser-ablated Co with O_2. [14] Such cluster was isolated in solid Ar, but was not detected in solid Ne or N_2. [14,35b] The present study revealed the non-planar cluster (CoOCo)O in ^1A state, which contains a three-member ring Co-O-Co

with a Co-Co bond and a terminal Co=O bond pointing out of the three-member ring plane, Figure 1. This isomer lies at 4.315 eV above the global minimum. The calculated harmonic frequency of 995 cm^{-1} for the stretching mode of the out-of-plane Co=O bond in this cluster, Table 5, agrees with the IR studies of Chertihin et al., in which a strong band at 944 cm^{-1} was assigned to the stretching vibration of a terminal cobalt-oxygen double bond. The only other cluster with a three-member ring, (CoOO)Co in ^{1}A' state, is found at 1.46 eV above the dissociation limit to 2Co + O_2. Based on differential spectra and force-constant calculations, Danset et al. [35b] reported Co_2O_2 species of low-symmetry, also containing three-member rings, which could not be confirmed by our study. The interactions with the matrix can be expected to play a major role in the stabilization of such species, though no coordination of noble-gas atoms could be inferred. The Co_2O_2 cluster reactivity is higher than that of the monomer CoO; it increases after carbonylation, as revealed by the values of the proton affinity, absolute negativity and hardness, Table 3. Both the ground-state dioxide complex $Co_2O_2(CO)_6$ and the antiferromagnetic low-spin dioxide complex in ^{3}A" and ^{1}A state respectively, have increased electron-donor capacity, evidenced by the high local charges on both Co and O centers, Table 2. The release of molecular oxygen from the hexacarbonyl complexes is more favorable compared to the bare clusters and the peroxide complex $Co_2(O_2)(CO)_6$ with side-on bonded dioxygen would dissociate O_2 in a weakly endothermic reaction. Strongly nucleophilic regions are formed in the vicinity of the oxygen atoms in both dioxides and peroxides, which in the carbonylated dioxides cover continuous area within the Co_2O_2 ring, Figure 10.

CONCLUSIONS

The DFT studies of clusters with Co_2O_2 stoichiometry reveal stabilization via antiferromagnetic coupling for the planar rhombic dioxide. Antiferromagnetic coupling stabilizes also the dications and the dianions of the dioxide, while the monocations and the monoanions have high-spin ground states. The local minima, corresponding to dioxides and peroxides with side-on bonded dioxygen have been

identified, all of them possessing planar rings and Co-Co bonds. The peroxo-isomers CoOOCo, in which largely separated Co atoms are bonded by a mid-positioned peroxo-bond, also have planar structure, but they are of lower stability than the rhombic dioxides and the peroxides with ring-structure. The dioxide has pronounced ionic features; the Co centers are strongly electrophilic and coordinate atoms from the inert-gas matrices, used in the IR studies. The peroxides are predominantly covalent. Large energy gaps separate the low-lying states of Co_2O_2 from the global minimum. Carbonylation stabilizes all clusters towards dissociation of the dimer and the energy gaps between low-lying states are reduced; their reactivity as electron-donors and nucleophilic reagents is increased due to the higher electron density induced in the vicinity of the Co_2O_2 rings.

Acknowledgment.

The computational results have been achieved using the Vienna Scientific Cluster (VSC). CPU time at the BG08-MADARA computer cluster, financially supported by project RNF01/0110 of the Bulgarian national science fund is also gratefully acknowledged.

SUPPORTING INFORMATION AVAILABLE. Tables with calculated molecular properties of the binuclear oxide, dioxide and peroxide clusters are included in Tables 1S-5S and Figures 1S-2S (9 pages). This information is available free of charge via the Internet at http://pubs.acs.org.

REFERENCES:

(1) (a) Limburg, J.; Vrettos, J. S.; Chen, H.; de Paula, J. C.; Crabtree, R. H.; Brudvig G. W. J. Am. Chem. Soc., **2001**, *123*, 423. (b) Beinert, H. J. Biol. Inorg. Chem., **2000**, *5*, 2. (c) Yeo, B. S.; Bell, A. T. *J. Am. Chem. Soc.*, **2011**, *133*, 5587.

(2) (a) Shirai, M.; Inona, T.; Onishi, H.; Asakura, K.; Iwasawa, Y. *J. Catal.*, **1994**, *145*, 159. (b) Parshall, G. W.; Ittel, S. D. Homogeneous Catalysis, J. Wiley & Sons: NY, **1992**. (c) Lopes, I.; Davidson, A.; Thomas C. *Catal. Commun.*, **2007**, *8*, 2105. (d) Solsona, B.; Vazquez, I.; Garcia, T.; Davies, T.; Taylor, S. *Catal. Lett.*, **2007**, *116*, 116.

(3) (a) Magnus, K. A.; Ton-That, H.; Carpenter, J. E. *Chem. Rev*., **1994**, *94*, 727. (b) Karlin, K. D.; Kaderli, S.; Zuberbühler, A. D. *Acc. Chem. Res.,* **1997**, *30*, 2239. (c) Nikolov, G. S.; Mikosch, H.; Bauer, G. *J. Mol. Str., (THEOCHEM)* **2000**, *499*, 35. (d) Flock, M.; Pierloot, K. *J. Phys. Chem. A*, **1999**, *103*, 95. (e) Gutsev, G.L.; Bauschlicher, C.W. *J. Chem. Phys*., **2003**, *119*, 3681 (f) Gutsev, G.L.; Bauschlicher, C.W. *J. Chem. Phys*., **2003**, *119*, 11135

(4) Catlow, C.R.A.; Bromley, S.T.; Hamad, S.; Mora-Fonz, M.; Sokol, A.A.; Woodley, S.M. *PCCP* **2010**, *12*, 786.

(5) Johnson, G. E.; Reveles, J. U.; Reilly, N. M.; Tyo, E. C.; Khanna, S.; Castleman, A. W. Jr. *J. Phys. Chem. A*, **2008**, *112*, 11330.

(6) Veliah, S.; Xiang, K.; Pandey, R.; Recio, J. M.; Newsam, J. M. *J. Phys. Chem. B* **1998**, *102*, 1126.

(7) Molek, K. S.; Anfuso-Cleary C.; Duncan M. A. *J. Phys. Chem. A*, **2008**, *112*, 9238.

(8) Klaassen J. J.; Jacobson, D. B. *J. Am. Chem. Soc*., **1988**, *110*, 974.

(9) Leopold, D. G.; Lineberger W. C. *J. Chem. Phys*., **1986**, 85, 51.

(10) Wang, H.; Khait, Y. G.; Hoffmann, M. R. Mol. Phys., **2005**, 103, 263.

(11) Ozaki, T.; Kino, N. *Phys. Rev. B* **2004**, *69*, 195113.

(12) Liu, L.; Zhao, R.-N.; Han, J.-G.; Liu, F.; Pan, G.-Q.; Sheng L.-S. *J. Phys. Chem. A*, **2009**, *113*, 360.

(13) Uzunova, E. L.; Nikolov, G. St.; Mikosch, H. *J. Phys. Chem. A*, **2002**, *106*, 4104.

(14) Chertihin, G. V.; Citra, A.; Andrews, L.; Bauschlicher, C. W. *J. Phys. Chem. A*, **1997**, *101*, 8793.

(15) (a) Yan, J.-Y.; Kung, H. H.; Sachtler, W. M. H.; Kung, M.C. *J. Catal.*, **1998**, *175*, 294. (b) Kung, H. Transition Metal Oxides: Surface Science and Catalysis, Studies in Surface Science and Catalysis vol. 45, Elsevier Sci. Ltd., **1991**. (c) Somorjai, G. A. Introduction to Surface Chemistry and Catalysis; John Wiley and Sons, New York, **1994**. (e) Teobald, B. J. *Tetrahedron* **2002**, *58*, 4133.

(16) Gaussian 09, Revision **C.01**, Frisch, M. J.; Trucks, G. W.; Schlegel, H. B.; Scuseria, G. E.; Robb, M. A.; Cheeseman, J. R.; Scalmani, G.; Barone, V.; Mennucci, B.; Petersson, G. A. et al. Gaussian, Inc., Wallingford CT, 2009.

(17) Becke, A. D. *J. Chem. Phys.* **1996**, *104*, 1040.

(18) (a) Adamo, C.; Barone, V. *Chem. Phys. Lett*., **1997**, *274*, 242. (b) Adamo, C.; Di Matteo, A; Barone, V. In *Adv. in Quantum Chemistry,* Sabin, J.; Löwdin, P.-O.; Lami, A.; Brändas, E. J.; Barone, V.; Sabin, J. R.; Zerner, M. C. Eds.; Academic Press: **1999**, *vol. 35-36*, p. 45.

(19) Lee, C.; Yang W.; Parr, R. G. *Phys. Rev.* **1988**, *B37*, 785-789.

(20) Miehlich, B.; Savin, A.; Stoll, H.; Preuss, H. *Chem. Phys. Lett.* **1989**, *157*, 200.

(21) Becke, A. D. *J. Chem. Phys.* **1993**, *98*, 5648.

(22) (a) Schwabe, T.; Grimme, S. *Phys. Chem. Chem. Phys.*, **2006**, *8*, 4398. (b) Schwabe, T.; Grimme, S. *Phys. Chem. Chem. Phys.*, **2007**, *9*, 3397.

(23) (a) Wachters, A. J. H. *J. Chem. Phys*., **1970**, *52*, 1033. (b) Hay, P. J. *J. Chem. Phys*., **1977**, *66*, 4377. (c) Raghavachari, K.; Trucks, G. W. *J. Chem. Phys*., **1989**, *91*, 1062.

(24) (a) Hay, P. J.; Wadt, W. R. *J. Chem. Phys.*, **1985**, *82*, 270. (b) Couty, M.; Hall, M. B. *J. Computational Chem.*, **1996**, *17*, 1359.

(25) (a) Lovell, T.; Himo, F.; Han, W.-G.; Noodleman, L. *Coord. Chem. Rev*. **2003**, *238*, 211. (b) Torres, R. A.; Lovell, T.; Noodleman, L.; Case, D. A. *J. Am. Chem. Soc.* **2003**, *125*, 1923. (c) Noodleman, L. *J. Chem. Phys.* **1981**, *74*, 5737.

(26) (a) Cizek, J. *Adv. Chem. Phys.* **1969**, *14*, 35. (b) Purvis, G. D.; Bartlett, R. J. *J. Chem. Phys.* **1982**, *76*, 1910. (b) Pople, J. A.; Krishnan, R.; Schlegel, H. B.; Binkley, J. S. *Int. J. Quant. Chem.* **1978,** *XIV*, 545. (c) Purvis, G. D.; Bartlett, R. J. *J. Chem. Phys.* **1982**, *76*, 1910.

(27) Tao, J. M.; Perdew, J. P.; Staroverov, V. N.; Scuseria, G. E. *Phys. Rev. Lett.*, **2003**, *91*, 146401.

(28) (a) Reed, A. E.; Curtiss, L. A.; Weinhold, F. *Chem. Rev.* **1988**, *88***,** 899. (b) Weinhold, F.; Carpenter, J. E. The Structure of Small Molecules and Ions, (Plenum, 1988)

(29) Merer, A. J. *Annual Rev. Phys. Chem.* **198**9, *40*, 407.

(30) Li, X.; Wang, L. S. *J. Chem. Phys.*, **1999**, *111*, 8389.

(31) (a) Huber, K. P.; Herzberg, G. Constants of Diatomic Molecules, van Nostrand Reinhold: New York, **1979**. (b) Comprehensive Handbook of Chemical Bond Energies, by Yu-Ran Luo, Taylor &

Francis, **2006**. (c) Ervin, K. M.; Anusiewicz, W.; Skurski, P.; Simons, J.; Lineberger, W.C. *J. Phys. Chem. A*, **2003**, *107*, 8521.

(32) Scheer, M.; Brodie, C.A.; Bilodeau, R.C.; Haugen, H.K. *Phys. Rev. A*, **1998**, *58*, 2051

(33) (a) Kant, A.; Strauss, B.J. *J. Chem. Phys*., **1964**, *41*, 3806. (b) Hales, D. A.; Su, C.-X.; Lian, L.; Armentrout, P. B. *J. Chem. Phys.*, **1994**, *100*, 1049 (c) Russon, L. M.; Heidecke, S. A.; Birke, M. K.; Conceicao, J. J.; Armentrout, P. B.; Morse, M. D. *Chem. Phys. Lett.*, **1993**, *204*, 235.

(34) (a) Uzunova, E. L.; Nikolov, G. St.; Mikosch, H. *ChemPhysChem* **2004**, *5*, 192. (b) Uzunova, E. L.; Mikosch, H.; Nikolov, G. St. *J. Chem. Phys.*, **2008**, *128*, 094307. (c) Uzunova, E. L. *J. Phys. Chem. A*, **2011**, *115*, 1320. (d) Uzunova, E. L. *J. Phys. Chem. A*, **2011**, *115*, 10665.

(35) (a) Staemmler, V.; Reinhardt, P.; Allouti, F.; Alikhani, M. E. *Chem. Phys*. **2008**, *349*, 83. (b) Danset, D.; Manceron, L. *PCCP*, **2005**, *7*, 583.

(36) Pearson, R. G. *Inorg. Chem.,* 1988, 27, 734.

(37) Zhan, C.-G.; Nichols, J. A.; Dixon, D. A. *J. Phys. Chem. A* **2003**, *107*, 4184.

(38) Hunter, E. P.; Lias, S.G. *J. Phys. Chem. Ref. Data*, **1998**, *27*, 413.

(39) (a) Lee, T.; Taylor, P. *Int. J. Quantum Chem.* **1989**, *23*, 199. (b) Lee, T., *Chem. Phys. Lett.*, **2003**, *372*, 362.

(40) (a) Sumner, G.G.; Klug, H.P.; Alexander, L.E. *Acta Cryst*. **1964**, *17*, 732. (b) Sweany R. L.; Brown, T. L. *Inorg. Chem.* **1977**, *16*, 415.

(41) (a) Lovallo, Chr.; Klobukowski, M. *Chem. Phys. Lett.*, **2003**, *368*, 589. (b) Bauschlicher, C. W.; Partridge, H.; Langhoff, S. R. *Chem. Phys. Lett*., **1990**, *165*, 272.

(42) Carnegie, P. D.; McCoy, A. B.; Duncan, M. A. *J. Phys. Chem. A*, **2009**, *113*, 4849.

(43) Carnegie, P. D.; Bandyopadhyay, B.; Duncan, M. A. *J. Phys. Chem. A*, **2011**, *115*, 7602.

(44) Bertini, L.; Bruschi, M.; de Gioia, L.; Fantuchi, P.; Greco, C.; Zampella, G. *Top Curr Chem* **2007**, *268*, 1.

Table 1. Bond Lengths, Bond Angles, Magnetic Moments on Atoms (μ, Bohr Magnetons) and Energies for the Ground States of the Dioxide $(CoO)_2$ and the Peroxo-isomers $Co_2(O_2)$, $Co(O_2)Co$ and CoOOCo [a]

Cluster Model	State	R_{Co-O} Å	R_{O-O} Å	R_{Co-Co} Å	∠OCoO ∠CoOO [b] deg	μ_{Co}	μ_{O}	ΔE_{tot}, eV B1LYP	ΔE_{tot}, eV CCSD(T)
Co_2O_2, D_{2h}	^1A	1.844	2.732	2.479	95.4	2.57 -2.57 [c]	0.00	**0.000**	**0.000**
	$^7\mathbf{B_{1u}}$	1.844	2.730	2.479	95.5	2.56	0.44	0.239	0.298
	$^7\mathbf{A_u}$	1.845	2.927	2.245	105.0	2.45	0.55	0.888	0.712
	$^5\mathbf{B_{3g}}$	1.805	2.826	2.247	103.0	2.10	-0.10	1.159	0.945
	$^3\mathbf{B_{3u}}$	1.798	2.652	2.426	95.1	1.42	-0.42	1.969	1.906
$[Co_2O_2]^{2+}$, D_{2h}	^1A	1.779	2.295	2.719	80.3	2.50 -2.50 [c]	-0.70 0.70	23.491	23.069
$[Co_2O_2]^{2-}$, D_{2h}	^1A	1.862	2.874	2.368	101.0	3.77 -3.77 [c]	0.00	1.457	1.370
$Co_2(O_2)$, C_{2v} [d]	$^7\mathbf{B_2}$	1.822	1.449	2.460	106.1	2.79	0.21	3.146	3.483
	$^3\mathbf{A_2}$	1.965	1.333	2.580	108.5	1.50	-0.50	4.141	4.894
	$^1\mathbf{A_1}$	1.729	1.420	2.116	101.6	0.00	0.00	6.085	4.862
$Co(O_2)Co$, C_{2v} [d]	$^7\mathbf{B_2}$	2.000	1.522	2.381	73.1	2.81	0.19	3.407	3.573

	$^5\mathbf{A_1}$	1.960	1.573	2.768	89.8	1.85	0.15	4.419	
CoOOCo, C_{2h}	$^5\mathbf{A_g}$	1.793	1.476		104.1	1.86	0.14	3.478	4.073
	$^3\mathbf{B_g}$	1.911	1.341		106.7	1.51	-0.51	5.226	6.147

[a] – a full list of the calculated local minima and their vibrational frequencies is available as Supporting Information in Tables 2S and 5S; [b] – ∠OCoO for dioxide clusters; ∠CoOO for peroxide clusters. [c] – broken-symmetry (BS) antiferromagnetic states, Figure 2; [d] – Figure 3. ΔE_{tot} – total energy difference relative to the ground state energy of neutral Co_2O_2: E_{tot} = -2915.891463 Hartree for B1LYP; zero-point correction included; -2913.306905 Hartree for CCSD(T).

Table 2. HOMO(SOMO)-LUMO gaps (eV) and natural charges (q_M, e) for neutral and charged $(CoO)_2$ species in antiferromagnetic (AFM) and in paramagnetic (PM) high-spin states, and for the peroxo-isomers $Co_2(O_2)$, and $Co_2O_2(CO)_6$.

Cluster	SOMO-LUMO	q_M	q_O	M 3d	M 4s
AFM states					
Co_2O_2	3.98	1.17	-1.17	7.35	0.27
$[Co_2O_2]^{2+}$	4.02	1.61	-0.61	7.36	0.11
$[Co_2O_2]^{2-}$	1.26	0.26	-1.26	7.55	0.74
$Co_2O_2(CO)_6$	4.31	-0.31	-0.72	7.89	0.38
PM, High-spin states					
Co_2O_2; $^7B_{1u}$	3.44	1.32	-1.32	7.36	0.28
$[Co_2O_2]^{2+}$; $^5B_{3g}$	3.68	1.52	-0.52	7.36	0.11
$[Co_2O_2]^{2-}$; ^7A_u	0.44	0.29	-1.29	7.55	0.74
$Co_2(O_2)$; $^7B_2$	2.66	0.63	-0.63	7.48	0.82
CoOOCo; ^5A_g	2.72	0.68	-0.68	7.62	0.66
$Co_2O_2(CO)_6$; $^3A''$	3.98	-0.31	-0.72	7.89	0.38
$Co_2(O_2)(CO)_6$; $^7A''$	2.28	-0.23	-0.27	7.89	0.43

Table 3. Calculated Proton Affinities (PA, kJ mol^{-1}), Absolute Electronegativities [a] (χ, eV), Hardness (η, eV) and Dissociation Energies (D_{zpe}, eV) [b] of the Ground State Dioxides Co_2O_2, $Co_2O_2(CO)_6$ and Peroxides $Co_2(O_2)$, $Co_2(O_2)(CO)_6$.

Cluster, Symmetry, State	PA	χ	η
Co_2O_2, D_{2h}; ^1A	827.0	5.79	5.19
$Co_2O_2(CO)_6$, C_s; ^3A"	1033.6	4.03	3.08
Co [a]		4.30	3.60
O [a]		7.54	6.08
C [a]		6.27	5.00
CO [c]		6.47	7.76
		D_{zpe}	
$(CoO)_2 \rightarrow 2Co + O_2$		5.83	
$(CoO)_2 \rightarrow 2CoO$		3.67	
$Co_2(O_2) \rightarrow 2Co + O_2$		2.68	
$Co_2(O_2) \rightarrow 2CoO$		0.52	
$Co_2O_2(CO)_6 \rightarrow 2Co + O_2 + 6CO$		8.89	
$Co_2O_2(CO)_6 \rightarrow 2CoO + 6CO$		6.73	
$Co_2O_2(CO)_6 \rightarrow Co_2(CO)_6 + O_2$		4.06	
$Co_2(O_2)(CO)_6 \rightarrow 2Co + O_2 + 6CO$		6.34	
$Co_2(O_2)(CO)_6 \rightarrow 2CoO + 6CO$		4.18	
$Co_2(O_2)(CO)_6 \rightarrow Co_2(CO)_6 + O_2$		1.51	

[a] ref. 36. [b] zero-point correction included; [c] ref. 37

Table 4: Bond Lengths, Bond Angles, Magnetic Moments on Atoms (μ, Bohr Magnetons), Spin Contamination Expectation Values ‹$\hat{S}^2$› and Energies for $Co_2O_2(CO)_6$ and $Co_2(O_2)(CO)_6$

Cluster Model	State	R_{Co-O} Å	R_{O-O} Å	R_{Co-Co} Å	R_{Co-C} Å	∠CoOCo ∠CoOO deg [a]	Dihedral ∠OCoOCo deg	μ_{Co}	μ_{O}	‹$\hat{S}^2$›	ΔE_{tot}, eV B1LYP
$Co_2O_2(CO)_6$	^{3}**A**"	1.853	2.456	2.724	1.88-2.00	94.6	16.3	1.00	-0.04	2.079	**0.000**
	^{1}**A**	1.853	2.456	2.732	1.89-2.00	95.0	14.8	1.05 -1.05 [b]	0.00		0.010
	^{5}**A**"	1.902	2.401	2.950	1.92-1.97	101.7	0.5	1.58	0.46	6.235	0.751
	^{7}**A**'	1.879	2.340	3.300	1.95-1.96	122.8	2.0	1.91	0.92	12.186	0.977
		2.191				97.7			1.32		
	^{1}**A**'	1.849	2.441	2.287	1.87-1.88	76.4	46.3	0.00	0.00	0.000	0.988
$Co_2(O_2)(CO)_6$	^{7}**A**"	2.100	1.321	3.180	1.95-1.97	116.3		2.19	0.54	12.082	2.545

[a] – ∠OCoO for dioxide clusters; ∠CoOO for peroxide clusters. [b] – broken-symmetry (BS) antiferromagnetic state, Figure 2c. ΔE_{tot} – total energy difference relative to the ground state energy of neutral $Co_2O_2(CO)_6$ with E_{tot} = -3595.844689 Hartree; zero-point correction included.

Table 5. Vibrational Frequencies and Zero-point Energies of the Ground state $(CoO)_2$ Clusters.

Cluster	State/ Symmetry	ω, cm^{-1}	ZPE, kJ mol^{-1}
Co_2O_2	^{1}**A**; **D_{2h}**	654 a_g 604 b_{2u} 496 b_{1u} 407 b_{3g} 278 a_g 216 b_{3u}	15.88
$Ar_4 + Co_2O_2$ [a]	^{1}**A**; **D_{2h}**	700; 634; 433; 398; 296; 261	17.75
$Ar_4 + Co_2O_2$ [a,b]	^{7}**B_{1u}**; **D_{2h}**	702; 684; 449; 393; 355; 264	18.51
Exp. in Ar [14]		685; 469; 304	
Exp. in Ne [14,35b]		684; 467; 293	
Exp. in N_2 [14]		706; 495	
Calc. [35]		708; 685; 469; 460; 293, 183	
$Ar_4 + Co_2(O_2)$ [c]	^{7}**B_2**	854; 525; 502	13.82
(CoOCo)O [d]	^{1}**A**, C_1	995; 754; 524; 209; 151; 98	16.33
Exp. [14]		944	
Exp. [35b]		839; 544; 530; 141	
(Co-OO)-Co [d]	^{1}**A'**, C_s	884; 640; 549; 370; 263; 133	16.97
Exp. [35b]		986; 950; 552	

[a,b] – $R_{(Co-Ar)}$ = 2.937 Å (B1LYP); 2.932 Å (B3LYP) [b] – $R_{(Co-Ar)}$ = 2.575 Å; 3.208 Å (B2PLYPD) [c] – $R_{(Co-Ar)}$ = 3.256 Å; $Co_2(O_2)$ in Ar is by 1.488 eV less stable than Co_2O_2. [d] – The structure is presented in Figure 1S (Supporting Information). The vibrational frequencies of other isomeric clusters and the ground-state carbonylated clusters are summarized in Table 5S (Supporting information).

Figure Captions

Figure 1. The ground states corresponding to the different isomeric Co_2O_2 clusters and low-lying local minima grouped according to spin multiplicity. Co atoms are small red circles, O atoms – large blue circles. The arrows denote the energy difference ΔE_{tot}, corresponding to adiabatic transitions (Zero-point corrections included). The three-member ring structures are displayed in detail in Figure 1S, as Supporting Information.

Figure 2. Spin magnetization density (SMD) distribution for a) Co_2O_2 b) $Co_2O_2^{2+}$ and c) $Co_2O_2(CO)_6$ in their broken-symmetry singlet states. Contour lines are at 3.5E-03 e a_0^3. Co atoms are red balls, O atoms – blue balls, C atoms – grey balls. Blue areas indicate surplus of α spin density and green areas – surplus of β density.

Figure 3. Rotation of O_2 perpendicular to the C_2-axis in $Co_2(O_2)$. Co atoms are red balls, O atoms – blue balls.

Figure 4. The symmetrical frontier orbitals of Co_2O_2: the $6b_{2u}$ SOMO, the $11a_g$ antibonding LUMO, Co-Co and Co-O bonding orbitals for a standard orientation of the rhombic planar cluster in the σ_{yz} plane and with the Co atoms lying along the z-axis. Positive parts of MOs are red, negative – green. Orbital energies, Hartree: $6b_{2u}$ (-0.2324), $11a_g$ (-0.1060), $10a_g$ (-0.3209), $9a_g$ (-0.3594), $8a_g$ (-0.4536), $7a_g$ (-0.9141).

Figure 5. Molecular Electrostatic Potential (MEP) maps of Co_2O_2, $Co_2(O_2)$ and CoOOCo clusters. Areas of positive EP (electrophilic) are yellow, the negative EP (nucleophilic) are displayed in blue.

Figure 6. Hexacarbonyl complexes of Co_2O_2 and $Co_2(O_2)$. Co atoms are light-red balls, O atoms – blue balls, C atoms – grey balls.

Figure 7. The SOMO, the Co-Co and Co-O bonding orbitals of $Co_2O_2(CO)_6$ in ^3A" state. Positive parts

of MOs are red, negative – green. Orbital energies, Hartree: 42a' (-0.2355), 40a' (-0.2677), 36a' (-0.3834), 35a' (-0.3975).

Figure 8. The bonding SOMO and the antibonding LUMO of $Co_2(O_2)(CO)_6$ in ^{7}A" state. Positive parts of MOs are red, negative – green. Orbital energies, Hartree: SOMO (-0.1566), LUMO (-0.0728).

Figure 9. Dicobalt dioxygen clusters, entrapped in the cubic unit cell of solid Ar. Ar atoms of the matrix are light blue, oxygen atoms – blue, transition metal center – red. a) the rhombic dioxide Co_2O_2; b) the planar peroxide with side-on bonded dioxygen $Co_2(O_2)$.

Figure 10. MEP maps of a) $Co_2O_2(CO)_6$ in ^{3}A" state and b) $Co_2(O_2)(CO)_6$ in ^{7}A" state. Areas of positive EP (electrophilic) are yellow, the negative EP (nucleophilic) are displayed in blue.

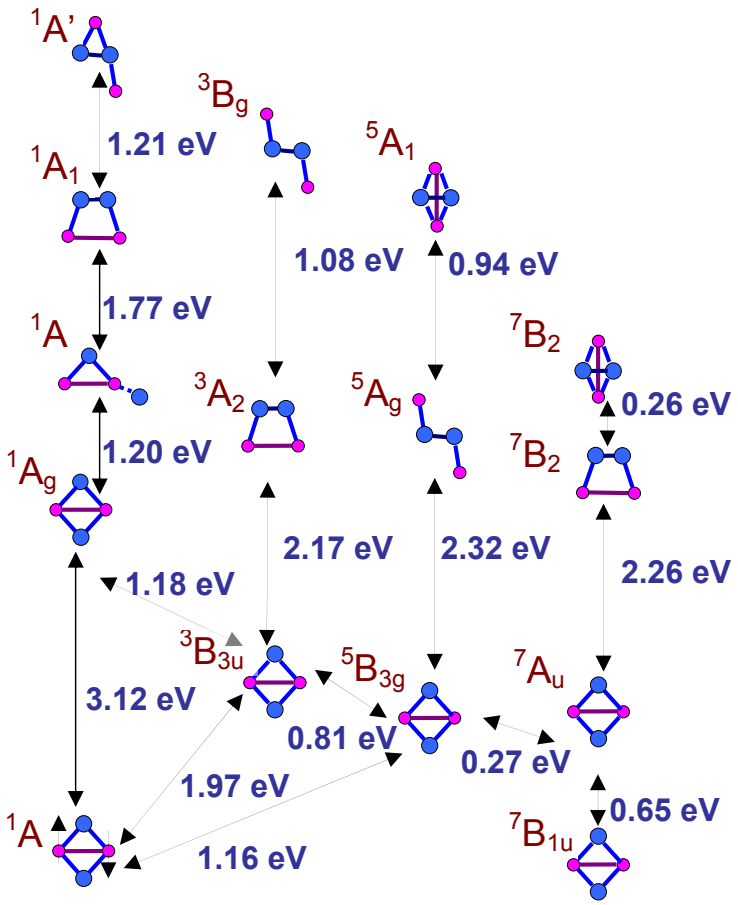
1A'
1.21 eV
1A1
1.77 eV
1A
1.20 eV
1Ag
1.18 eV
3.12 eV
1A
1.97 eV
1.16 eV
3Bg
1.08 eV
3A2
2.17 eV
3B3u
0.81 eV
5A1
0.94 eV
5Ag
2.32 eV
5B3g
0.27 eV
7B2
0.26 eV
7B2
2.26 eV
7Au
0.65 eV
7B1u

Figure 1

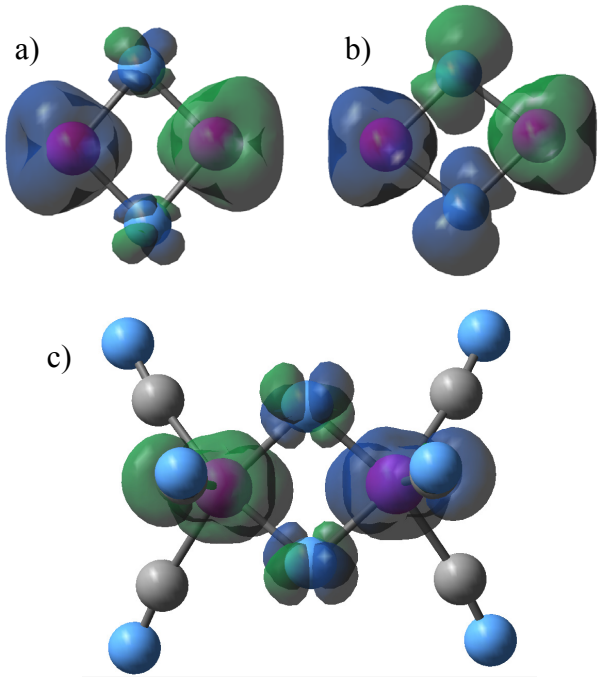

Figure 2

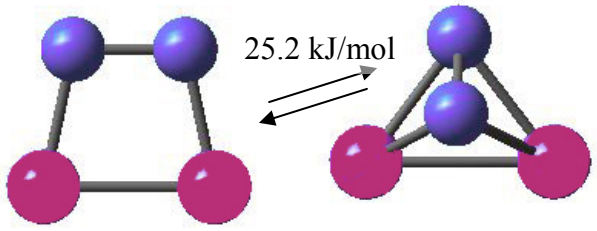

Figure 3

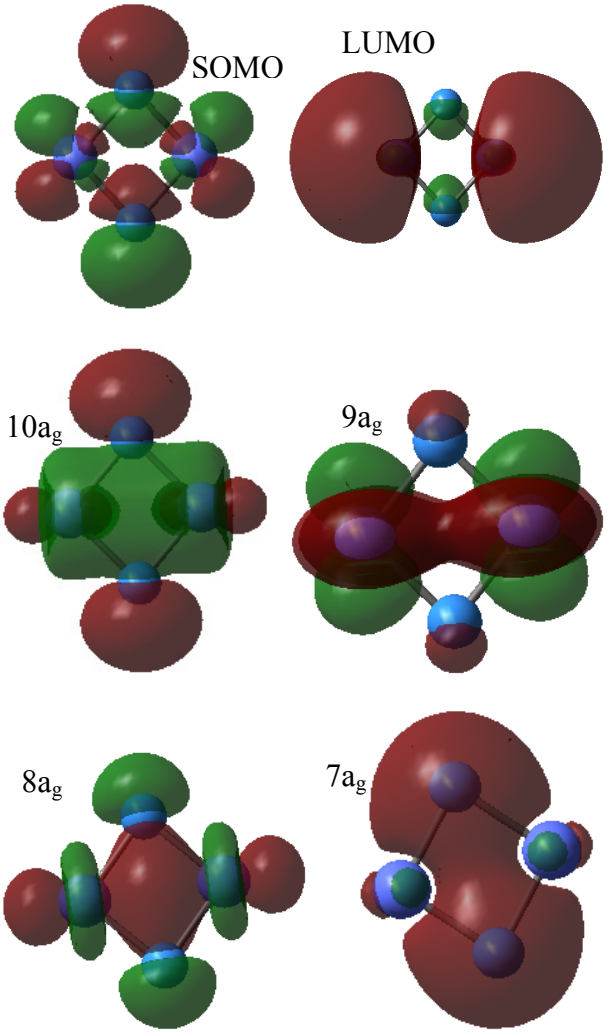

Figure 4

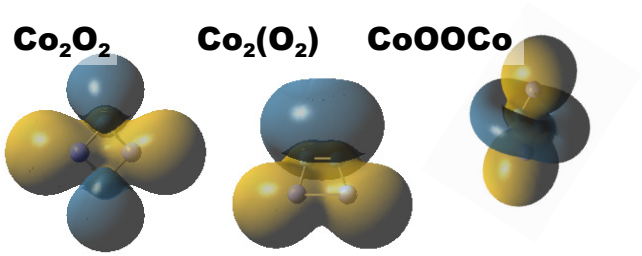

Figure 5

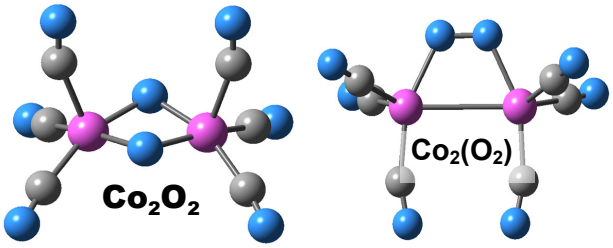

Figure 6

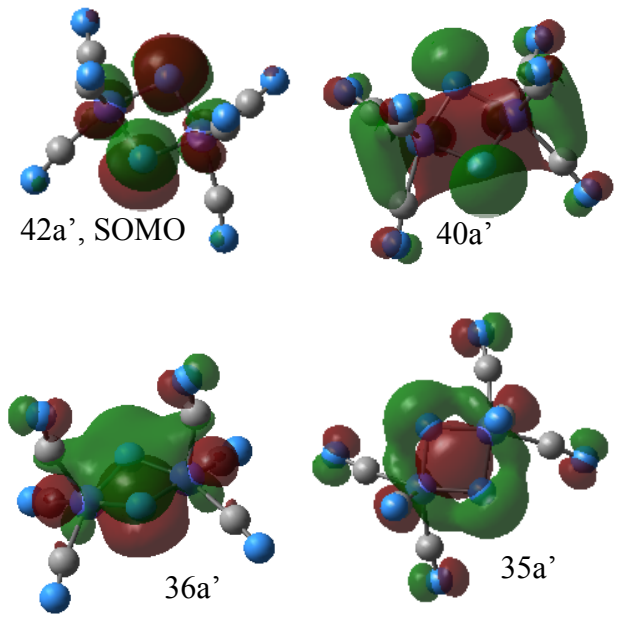

Figure 7

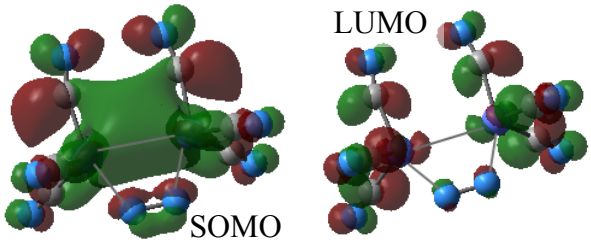

Figure 8

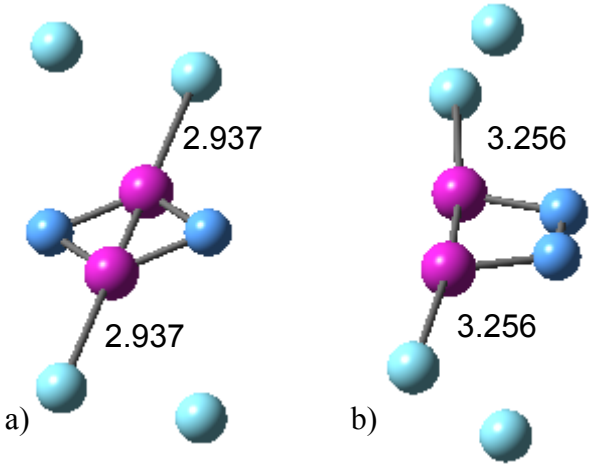

Figure 9

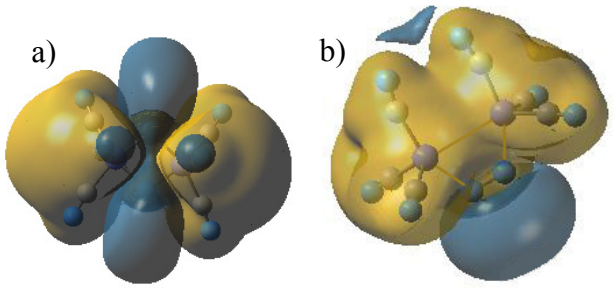

Figure 10

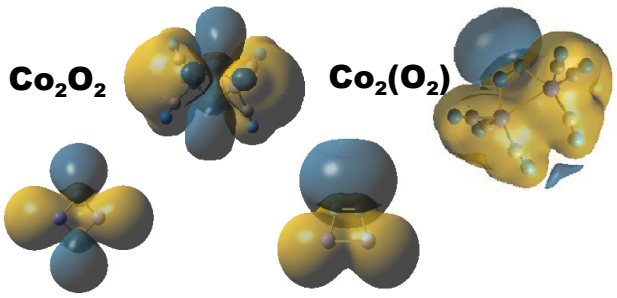

TOC graphic